Thermophoretic and Evaporational Losses of Ultrafine Particles in Heated Flow

Manabu Shimada, Takafumi Seto, and Kikuo Okuyama
Dept. of Chemical Engineering, Hiroshima University, Higashi-Hiroshima 724, Japan

The transport, wall deposition and evaporation of nanometer-sized aerosol particles are studied using a nonisothermal laminar flow in a pipe. The test aerosol particles, monodisperse Ag and NaCl particles of 7–40 nm dia., are introduced into a vertical circular pipe with wall temperature distribution in the axial direction. The measured particle loss during transport through the pipe increased with the wall temperature difference. The enhancement of particle loss due to diffusive and thermophoretic deposition is examined by the gas flow, temperature, and particle concentration distribution equations. Predicted particle losses agreed with the experimental results when the local variation of gas properties, particle Brownian diffusion, and thermophoretic migration are considered. Sudden increases in the particle loss due to particle evaporation were also observed at very high temperatures (about 700°C for Ag particles and 400°C for NaCl particles). The measured reductions of particle diameter due to evaporation showed good agreement with calculation based on aerosol evaporation theory for free-molecule regime.

Introduction

In the production of fine particles in gas, particle deposition on the walls of the chamber or tube in which the particles are synthesized often reduces product yield substantially. An understanding of the particle behavior in heated or cooled flows is important for the design of particle and thin film synthesis reactors, such as the manufacture of lightguide preforms by modified chemical vapor deposition, production of TiO_2 pigment powders, as well as a system for sampling from high temperature gases using tube probes. Such nonisothermal transport of gas/fine particle systems is also encountered in many other situations including hot gas and fly ash in liquid fuel and coal combustion, and impurities or products from wall attrition in heat exchangers. Particle deposition in some processes should be prevented since it causes reduced efficiency of production or blockade of channels and nozzles, but in some processes conditions for high deposition efficiency are desired to obtain high process yields.

The dynamics of nonisothermal particle-laden gas systems are affected by following various interrelated heat and mass transport phenomena: particle diffusion, convective heat transfer, mass transfer in noncontinuum range, nonuniform heating and fluid flow, and nonuniform forces acting on particles. For transport and deposition of particles, effects of Brownian diffusion, gravitational sedimentation, and thermophoretic migration are important. While Brownian diffusion and sedimentation have been extensively studied, the latter mechanism has not been fully clarified for ultrafine particles. The reason for this is that an experimental investigation for thermophoresis alone is almost impossible for nanometer-sized particles with large Brownian diffusivity. Therefore, the combined effects of nonisothermal convection, nonuniform thermophoretic migration and Brownian diffusivity are very important but have not been made sufficiently clear. There have been very few experiments with sufficient accuracy using nanometer-sized particles and nonisothermal flow because of difficulties in generation and measurement of particles tested. Heating or cooling of gas also causes change of particle properties due to particle evaporation and condensation. These are also important but are not yet fully explained especially for small solid particles.

Particle transport by thermophoresis in laminar flows has been studied by a considerable number of investigators. Walker et al. (1979) derived an analytical expression for particle deposition by thermophoresis and Brownian diffusion in a pipe

Correspondence concerning this article should be addressed to M. Shimada.

with a sudden decrease in wall temperature at a given axial position. Extension of the theoretical approach to simultaneous particle coagulation, diffusion and thermophoresis was made by Pratsinis and Kim (1989), who presented nomographs for particle deposition efficiency in dimensionless form. Stratmann and Fissan (1988) modeled the particle transport in cooled tube flows and presented numerical calculation results in which the local variation of the Brownian diffusivity and the gas properties such as viscosity and heat conductivity were taken into consideration.

There are rather few experimental verifications of the existing theories for nonisothermal laminar flows. Stratmann and Fissan (1989) measured the deposition of particles, 30–100 nm in diameter, using a circular pipe with walls cooled to 0°C and compared the results with an extended theory. Montassier et al. (1991), who used a similar experimental apparatus to Stratmann and Fissan, collected data covering a large range of particle sizes (ranging from 0.05- to 8-μm in diameter) and compared the data with a simple model.

In the aforementioned experiments, the test aerosols were heated at a maximum of 100°C. There have been very few measurements for the larger temperature differences (for example, several hundreds degrees per centimeters) that are often encountered in aerosol reactors. Furthermore, experiments on smaller particles are thought to be still insufficient.

Measurement of particle size for aerosols flowing through pipes heated at several hundred degrees was performed by Schmidt-Ott (1989). He investigated the effect of heating on the morphology of randomly-shaped agglomerates composed of nanometer-sized primary particles, but did not address the transport of particles. There have been numerous studies on evaporation of liquid aerosol particles including a recent study of Rader et al. (1987), who presented the method for measuring the evaporation rates of very fine droplets of 0.02–0.2 μm using two differential mobility analyzers. However, no work is found in which the evaporative loss of initially solid particles is investigated systematically.

The primary objective of this study is to present the effect of a nonisothermal flow field on the depositional and evaporative loss of nanometer-sized aerosol particles. The particle loss in a circular pipe heated by furnaces up to 950°C is measured using test aerosol particles, monodisperse Ag and NaCl particles of 7–40 nm in diameter. The combined effects of convection, diffusion and thermophoresis in nonisothermal flow is discussed at first. The measurements are compared with the theoretical calculations in which the equations for gas flow, temperature and particle distribution accounting for Brownian diffusion and thermophoretic migration are solved numerically. The evaporative loss of particles observed in terms of particle size reduction is also investigated with the theory for particle evaporation in free-molecule regime.

Loss of Ultrafine Particles in a Partially Heated Pipe

Figure 1 is a schematic illustration of the circular test pipe analyzed in this study, together with the behavior of ultrafine particles inside the pipe. A gas stream containing the particles is introduced at the pipe inlet ($z=0$) at a volumetric flow rate Q. The flow is heated by electrical furnaces around the pipe. Due to this heating, the gas velocity and physical properties

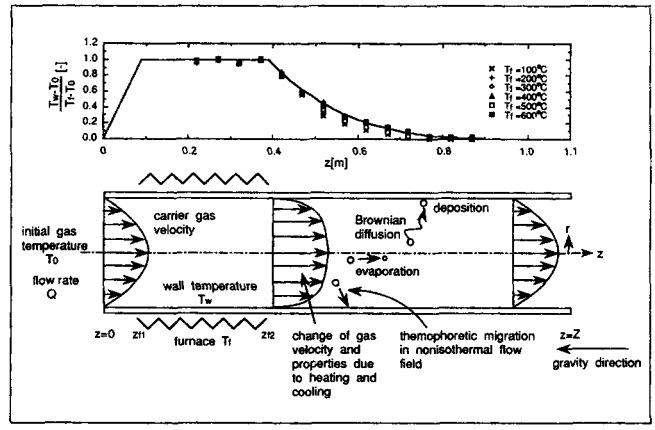

Figure 1. Circular test pipe and behavior of particles in the pipe.

change as it flows inside the pipe. The particles entrained in the gas are transported by the gas stream, and some of them are lost by diffusive deposition on the inner walls. Due to the temperature variations in the pipe, the Brownian diffusion coefficient of particles will vary with position, and particles will migrate by thermophoretic transport away from hot flow regions toward colder regions. Furthermore, solid particles may evaporate when the temperature is very high.

The governing equations of the gas velocity and temperature are the following:

Equation of Continuity:

$$\frac{1}{r}\frac{\partial}{\partial r}(r\rho u)+\frac{\partial}{\partial z}(\rho v)=0 \tag{1}$$

Radial (r-Direction) Momentum Equation:

$$\frac{1}{r}\frac{\partial}{\partial r}(r\rho uu)+\frac{\partial}{\partial z}(\rho vu)=\frac{1}{r}\frac{\partial}{\partial r}\left(\frac{4}{3}r\mu\frac{\partial u}{\partial r}\right)+\frac{\partial}{\partial z}\left(\mu\frac{\partial u}{\partial z}\right)$$
$$-\frac{2u}{3r}\left(\frac{2u}{r}+\frac{\partial\mu}{\partial r}\right)-\frac{3}{2}\frac{\partial}{\partial r}\left(\mu\frac{\partial v}{\partial z}\right)+\frac{\partial}{\partial z}\left(\mu\frac{\partial v}{\partial r}\right)-\frac{\partial p}{\partial r} \tag{2}$$

Axial (z-Direction) Momentum Equation:

$$\frac{1}{r}\frac{\partial}{\partial r}(r\rho uv)+\frac{\partial}{\partial z}(\rho vv)=\frac{1}{r}\frac{\partial}{\partial r}\left(r\mu\frac{\partial v}{\partial z}\right)+\frac{\partial}{\partial z}\left(\frac{4}{3}\mu\frac{\partial v}{\partial z}\right)$$
$$+\frac{1}{r}\frac{\partial}{\partial r}\left(r\mu\frac{\partial u}{\partial z}\right)-\frac{2}{3r}\frac{\partial}{\partial z}\left\{\mu\frac{\partial}{\partial r}(ru)\right\}-\frac{\partial p}{\partial z}+\rho g \tag{3}$$

Energy Equation:

$$\frac{1}{r}\frac{\partial}{\partial r}(r\rho C_pTu)+\frac{\partial}{\partial z}(\rho C_pTv)=\frac{1}{r}\frac{\partial}{\partial r}\left(rk\frac{\partial T}{\partial r}\right)$$
$$+\frac{\partial}{\partial z}\left(k\frac{\partial T}{\partial z}\right)+\rho T\left(u\frac{\partial C_p}{\partial r}+v\frac{\partial C_p}{\partial z}\right) \tag{4}$$

In Eqs. 1-4, u and v are the radial and axial velocity components, p and T are the pressure and temperature, μ, C_p, k

and ρ are the viscosity, specific heat, thermal conductivity and density of the gas, respectively. ρ is assumed to obey the following ideal gas law

$$\rho = pm_j/\kappa T \tag{5}$$

where m_j is the mass of a gas molecule and κ is the Boltzmann constant.

The boundary conditions of Eqs. 1-4 are:

$$z=0,\ 0\le r<R;\quad T=T_0,\ v=\frac{2Q}{\pi R^2}\left\{1-\left(\frac{r}{R}\right)^2\right\},\ u=0 \tag{6}$$

$$0<z\le z_{f1},\ r=R;\ T=T_w=T_f+(T_0-T_f)\frac{z_{f1}-z}{z_{f1}},\ v=u=0 \tag{7}$$

$$z_{f1}<z\le z_{f2},\ r=R;\ T=T_w=T_f,\ v=u=0 \tag{8}$$

$$z_{f2}<z\le Z,\ r=R;\ T=T_w=T_0+(T_f-T_0)\left(\frac{Z-z}{Z-z_{f2}}\right)^a,\quad v=u=0 \tag{9}$$

$$z=Z,\ 0\le r<R;\ \partial T/\partial z=0,\ \partial v/\partial z=0,\ u=0 \tag{10}$$

where R and Z are the inner radius and length of the pipe, z_{f1} and z_{f2} are the positions of the ends of the heated furnaces, and T_w is the wall temperature.

The symbols in the graph of Figure 1 show the relationship between the furnace temperature T_f and the wall temperature profile. The boundary conditions for wall temperatures, Eqs. 7-9, are approximate expressions based on the temperatures actually measured with a thermocouple and the experimental apparatus described later. A good approximation of the temperature distribution was found when the value of a in Eq. 9 was set to be 4.

The steady-state transport of aerosol particles flowing in a pipe is generally affected by diffusion of particles, gravitational and inertial forces, and external forces such as electric and thermophoretic forces. Forces due to gravity and particle inertia, however, are usually not important for particles smaller than 0.1 μm. The influence of electric forces is also excluded in the present analysis. For nonuniform temperature and velocity profiles, the governing equation of particle number concentration n [particles/kg of carrier gas] is given by:

Convection-Diffusion Equation:

$$\frac{1}{r}\frac{\partial}{\partial r}\{r\rho(u+v_{Tr})n\}+\frac{\partial}{\partial z}\{\rho(v+v_{Tz})n\} =\frac{1}{r}\frac{\partial}{\partial r}\left(r\rho D\frac{\partial n}{\partial r}\right)+\frac{\partial}{\partial z}\left(\rho D\frac{\partial n}{\partial z}\right) \tag{11}$$

The diffusivity of a particle, D, is given by the Stokes-Einstein equation:

$$D=\frac{\kappa T}{3\pi\mu d_P}C_c \tag{12}$$

where d_p is the particle diameter, and C_c, the Cunningham correction factor, is expressed by a function of particle Knudsen number, $Kn=2\lambda/d_p$, as (Davies, 1945):

$$C_c=1+Kn\{1.257+0.40\exp(-1.10/Kn)\} \tag{13}$$

The mean free path of the gas molecules, λ, is:

$$\lambda=\frac{\kappa T}{\sqrt{2}\pi\sigma_{jj}^2 p} \tag{14}$$

where the collision diameter, σ_{jj}, is 0.380 nm for N_2 molecules (Reid et al., 1986).

v_{Tr} and v_{Tz} in Eq. 11 are the thermophoretic velocities which result from the temperature nonuniformity. According to Talbot et al. (1980), they have the following form:

$$v_{Tr}=-\alpha\frac{\mu}{\rho}\frac{\partial \ln T}{\partial r},\ v_{Tz}=-\alpha\frac{\mu}{\rho}\frac{\partial \ln T}{\partial z} \tag{15}$$

$$\alpha=2.294\times\frac{\{(k/k_p)+2.20Kn\}[1+Kn\{1.2+0.41\exp(-0.88/Kn)\}]}{(1+3.438Kn)\{1+2(k/k_p)+4.40Kn\}} \tag{16}$$

where α is the thermophoretic coefficient and k_p is the thermal conductivity of the particle.

The boundary conditions for particle distribution, Eq. 11, are given as:

$$z=0,\ 0\le r<R;\ n=n_i \tag{17}$$

$$0\le z\le Z,\ r=R;\ n=n_w \tag{18}$$

In these boundary conditions, n_i is the particle concentration at the inlet and n_w is the concentration on the wall surface. The value of n_w can be set to zero if a particle is immobilized immediately after arrival on a surface and can never be borne by the gas stream again.

All the equations are transformed into finite difference formulae using a control volume method and are solved by the SIMPLER algorithm (Patankar, 1980). The dependences of properties of N_2 gas such as μ, C_p and k on temperature are estimated by the method described by Reid et al. (1986). After comparisons were made among numerical solutions with different grid sizes, most of the calculations were performed with 20 radial grids and 60 axial grids.

Experimental Apparatus and Method

The apparatus used in the experiments consists of an aerosol generator, a vertically-standing test pipe, differential mobility analyzers, and condensation nucleus counters, as shown in Figure 2. The evaporation-condensation type aerosol generator can quite stably produce ultrafine aerosol particles of Ag and NaCl suspending in N_2 gas. The resulting particle-size distribution has a geometric standard deviation of about 1.4. The number concentration is typically 10^{11}-10^{13} particles/m^3. This polydisperse aerosol is fed into the first differential mobility analyzer (DMA, TSI Inc., Model 3071). The classified aerosol drawn from the DMA, the particle number concentration and

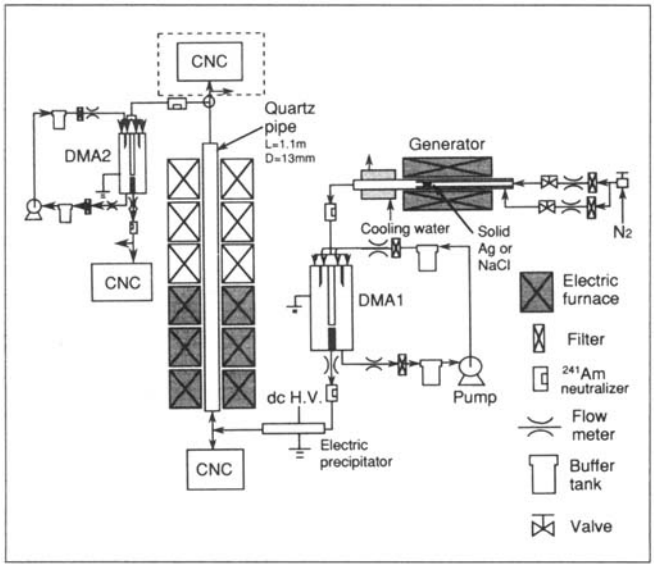

Figure 2. Experimental apparatus for measuring particle loss in test pipe.

standard deviation of particle size of which respectively are less than 5×10^9 particles/m^3 and 1.2, is passed through an Am-241 neutralizer in order to bring the aerosol particles to the equilibrium charging state by exposure to bipolar ions. The aerosol is then passed through an electrical precipitator consisting of parallel dc electrodes. The uncharged test aerosol obtained is divided into two lines with a Y-shaped connector, and the lines are connected with short silicon rubber tubes to the quartz test pipe and the first condensation nucleus counter (CNC, TSI Inc., Model 3020) to feed the aerosol continuously.

The test section, a cylindrical pipe of 1.1 m in length and 13 mm in diameter, is equipped with six electric furnaces around it. The temperature of each of the 0.1 m long furnaces is independently controlled. In the present experiments, only the lower three of the six furnaces are heated to T_f. This results in the wall temperature profile shown in Figure 1. The range of average gas velocities, $\bar{v}$, and Reynolds numbers, Re $[=(2R)\bar{v}\rho/\mu]$, at the pipe inlet is between 3.8×10^{-2} and 2.5×10^{-1} m/s, and 35 and 230, respectively.

After the test aerosol exits the test pipe, the particle number concentration and particle-size distribution are measured by the second CNC (TSI Inc., Model 3025) and the second DMA. The analyzer column of this DMA is shorter in length than the first one, which has been described in detail by Kousaka et al. (1986). This, combined with the improved performance of the Model 3025 CNC, improves the efficiency with which the small particles are counted. The second CNC is directly connected to the outlet of the test pipe when the change in the particle number concentration between the inlet and outlet is measured. The difference in the counting efficiencies between the two CNCs were corrected based on preliminary experiments where both CNCs were connected in parallel upstream of the test pipe simultaneously. The CNC measurements determine the number of particles in a unit gas volume. Since the difference between the gas temperature at the pipe exit and that at the inlet (283 ± 10 K) was less than 5 K, the volumetric flow rates of the gas at the inlet and the exit differ by only a few percent. Hence, the two measurements are directly comparable.

The ratio of particle number concentration at the pipe outlet to that at the inlet (penetration, P) is given as $P=n_o^*/n_i^*$, where n_o^* and n_i^* respectively are the particle number concentrations in a unit volume obtained by the CNCs at the outlet and inlet.

Measurement of the particle-size distribution at the pipe outlet is made by inserting the second DMA prior to the second CNC. The number concentration of the classified aerosol is measured to obtain the electric mobility distribution. The particle-size distributions are determined by converting the mobility distributions using Hoppel's method where the stationary bipolar charge distribution from the bipolar charging theory of Fuchs is used (Adachi et al., 1990).

Experimental Results and Comparison with Calculations

Determination of velocity and concentration profiles at pipe entry

Figure 3 shows the penetration of aerosol particles, P, measured for various particle sizes at the pipe inlet, d_{pi}. When the furnace around the pipe is not heated ($T_f=10$°C), that is, when the gas temperature is uniform across the pipe, wall loss of particles increases with decreasing particle diameter because the transport of particles onto the pipe wall is governed solely by Brownian diffusion. Accordingly, the penetration becomes smaller as the particle size decreases. The solid lines in the figure are the values of P calculated by substituting the solution of particle distribution from Eq. 11 into:

$$P=\frac{\int_0^R n(r,Z)\rho(r,Z)v(r,Z)2\pi r dr}{\int_0^R n(r,0)\rho(r,0)v(r,0)2\pi r dr} \tag{19}$$

Although the velocity distribution at the pipe inlet cannot be measured, a fully developed velocity profile as described by Eq. 6 was assumed in the calculation of solid lines. To check the validity of the assumption, additional calculations in which the inlet velocity profile is taken to be uniform were carried out. It is shown in the figure that the calculated results (dotted lines) are virtually the same as the solid lines. The fact that the velocity profile at the pipe inlet has almost no influence on penetrations suggests very short distance of velocity developing regions. An estimation of the length of the developing region is given by 0.07 RRe according to Bird et al. (1960), and the Reynolds numbers for the experiments for measuring P ($Q=0.3$ to 1 l/min) give the short distance ranging from 16 to 52 mm.

The particle concentration profile at the inlet is also very difficult to be measured. If we assume a limiting situation that the concentration profile is fully developed, the profile can be estimated analogically from the solution of the Graetz problem. Taking only the first term of the infinite series solution because a sufficiently large value of the axial coordinate is assumed, the shape of inlet profile is expressed as $n_i \propto \phi_0(r/R)$, where the value of ϕ_0 is tabulated in a literature (for example, Knudsen and Katz, 1958).

The penetrations assuming the developed concentration pro-

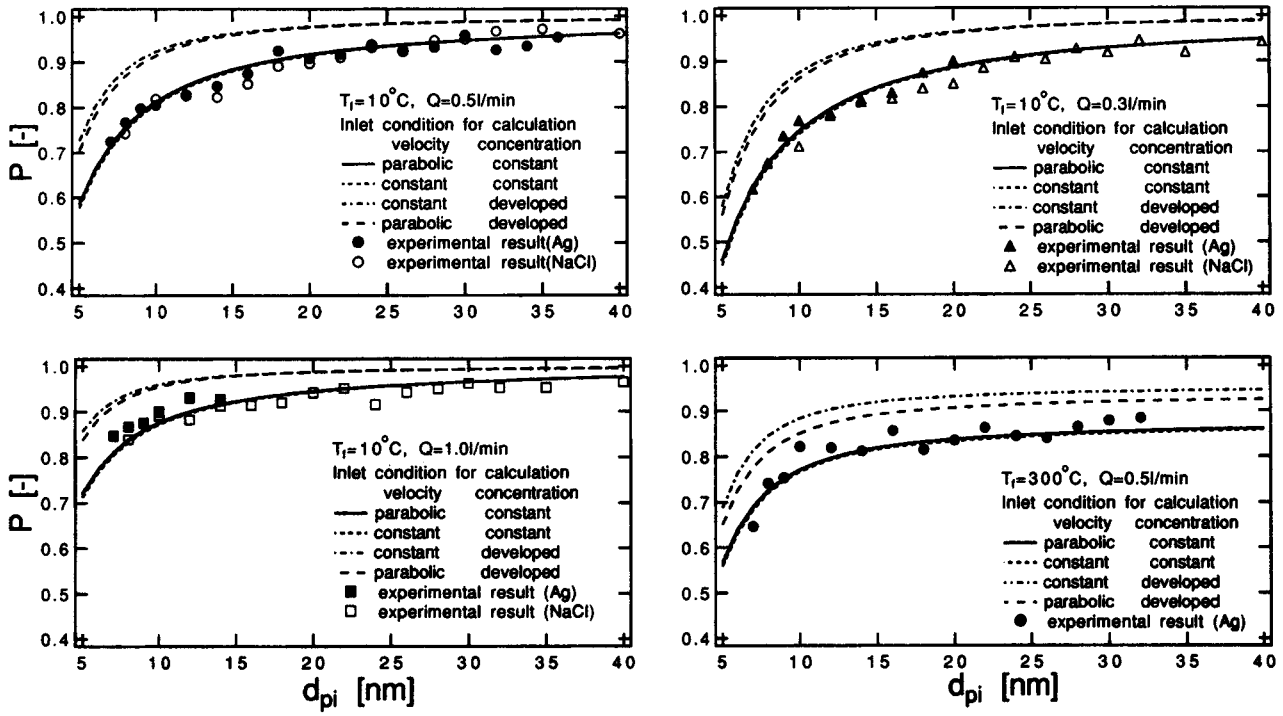

Figure 3. Penetration of particles, P, against particle diameter, d_{pi}, for isothermal flow (T_f= 10°C) and nonisothermal flow (T_f= 300°C).

file are shown by the chained and dashed lines. While the measured penetrations agree well with the prediction where the concentration profile is assumed to be uniform (solid and dotted lines) as described, there are significant deviations between the measurements and the prediction based on the developed concentrations. Consequently, the inlet concentration is considered to be uniform. It is reasonable, because the order of magnitude of Schmidt number ($\mu/\rho D$) is from 10^2 to 10^3

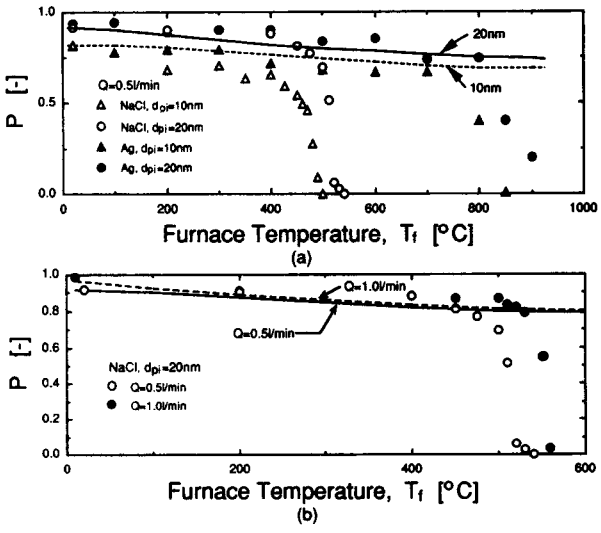

Figure 4. Penetration of particles, P, against furnace temperature for nonisothermal laminar flow.

Solid and dashed lines indicate results from present calculation: (a) effect of particle size and material; (b) effect of flow rate of gas.

and the development of particle concentration is very much slower than that of fluid velocity.

In addition, both the present measurements and calculations for isothermal flow agreed well with the analytical solutions for penetration (Gormley and Kennedy, 1949) in which parabolic velocity profile and uniform concentration at the inlet are assumed. The present calculations coincided with the analytical solutions with an accuracy of 0.6%. From the above discussion, the profiles of flow velocity and particle concentration at the test pipe inlet can be assumed as parabolic and uniform, respectively. And the agreement between measurements and both numerical and analytical calculations also indicates that the loss of particles in the other pipe lines except the test pipe is almost negligible.

Furthermore, the numerical calculation results are obtained by setting $n_w = 0$ in the boundary condition for particle concentration, Eq. 18. The close agreement between the measured and predicted penetration indicates that a particle once arriving at a wall surface is immediately immobilized and will no longer be entrained into the carrier gas.

Particle penetration at elevated temperatures

Figures 4a and 4b shows the particle penetrations obtained at elevated temperatures of the furnaces. When the furnace temperature is relatively low (<700°C for Ag particles and <400°C for NaCl particles), the change in P with T_f shows essentially the same tendency for Ag and NaCl particles. The penetration gradually decreases with T_f, indicating that the wall loss is enhanced with T_f. The solid and dashed lines in the figure are the calculation results by Eqs. 11 and 19. The difference in the results for Ag and NaCl particles were so little that they could not be distinguished in the figure, since

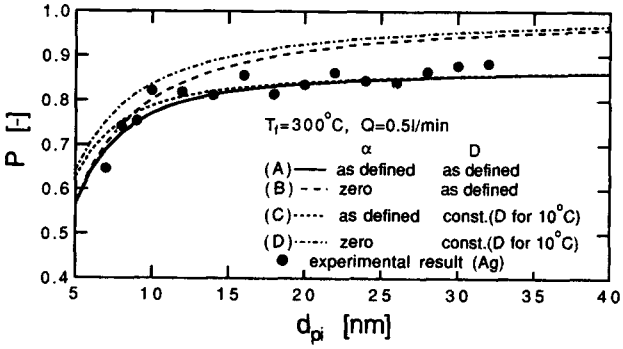

Figure 5. Penetration of particles, P, against particle diameter, d_{pi}.

Line A is the result of present calculation, Line B is the result calculated by neglecting the thermophoretic migration, Line C by setting Brownian diffusion coefficient to be constant and Line D by neglecting both thermophoretic migration and local variation of Brownian diffusivity. The furnace temperature, T_f, is 300°C.

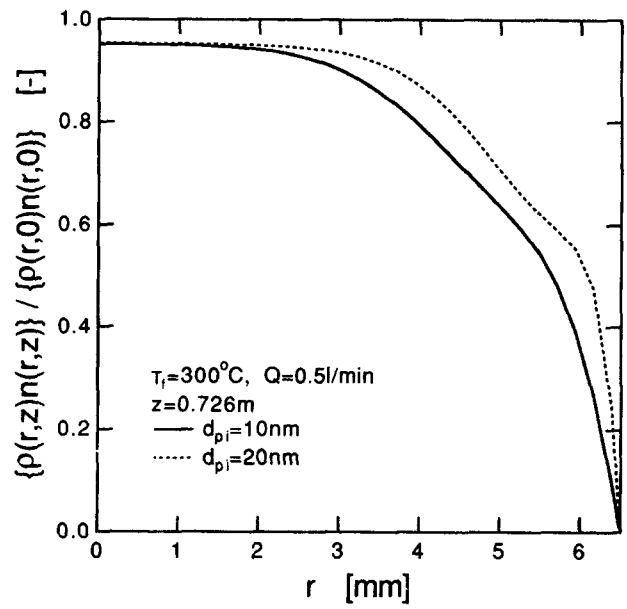

Figure 6. Particle concentration profile in a section of pipe for furnace temperature of 300°C.

the values of the thermophoretic coefficient, α, were almost the same for both materials. The main reason for this is that the particle size is very small and, thus, the Knudsen number Kn in Eq. 16 is orders of magnitude larger than k/k_p. The solid and dashed lines explain the experimental results obtained within the lower temperature region described above.

To investigate the reasons for decreased penetration with increasing furnace temperature, additional calculations were performed to examine the effects of thermophoretic force and spatial distribution of Brownian diffusivity due to temperature nonuniformity. The solid line A in Figure 5 shows the present calculation results, whereas the dashed line B presents the results calculated by neglecting the thermophoretic migration of particles, the dotted line C represents those obtained by setting Brownian diffusion coefficient to be a constant value (the value at the pipe inlet) throughout the inner space of the pipe, and the chain line D presents those obtained by both neglecting thermophoresis and temperature (and thus spatial) dependence of Brownian diffusivity.

The measured penetrations for Ag particles are plotted in the figure. The solid line lies the closest to the measured penetrations among the four lines, while the other lines underestimate the particle losses. The deviation between lines A and C (or lines B and D) indicates that the dependence of Brownian diffusion coefficient on gas temperature and viscosity, as described by Eq. 12, influences the wall loss when the particle size is small. This figure also reveals that the thermophoretic effect which is illustrated by the deviation between the solid and dashed lines is predominant for the enhancement of the wall loss of particles. Thermophoretic coefficient, α, and thus thermophoretic velocity, v_{Tr} and v_{Tz}, in Eqs. 15 and 16 are found to have almost no dependence on particle size. Accordingly, the deviation between the solid and dashed lines (lines A and B) in Figure 5 would be independent of particle size if the effect of thermophoretic deposition could be simply superposed on diffusive deposition. However, the deviation is smaller for smaller particle size. This trend in the deviation can be explained by considering the combined effects of Brownian diffusion and thermophoresis on particle concentration profile.

Figure 6 describes calculated concentration profiles as a function of radial position for two different particle sizes. The profile for larger particles (d_{pi} = 20 nm) exhibits a steeper concentration decrease near the pipe wall (r = 6.5 mm) than that for smaller particles (d_{pi} = 10 nm). In other words, the particle concentration in the vicinity of the wall is higher for larger particle size. Since thermophoretic particle flux towards the wall is proportional to the concentration above the wall as well as the thermophoretic velocity, the effect of thermophoretic deposition is less significant for smaller particles. Accordingly, the deviation between the solid and dashed lines is considered to become smaller with decreasing particle size.

The change in deposition rates in the axial direction of the test pipe is also predicted from the present numerical solutions. The number of particles depositing between the axial positions z and $z+\Delta z$ (area: $2\pi R\Delta z$) is expressed as $-\Delta(\int_0^R n\rho(v+v_{Tz})2\pi r dr)$. Then the number of particles depositing per unit area and time (particle flux) is:

$$\frac{-d\left[\int_0^R n\rho(v+v_{Tz})2\pi r dr\right]}{2\pi R dz} = -\frac{1}{R}\frac{d}{dz}\int_0^R n\rho(v+v_{Tz})r dr \qquad (20)$$

The particle flux can be normalized by the uniform concentration at the pipe inlet, $n_i\rho_i$ (particles/m^3) since the particle flux is proportional to the inlet concentration. The normalized deposition rate, K, is expressed by:

$$K = -\frac{1}{n_i\rho_i R}\frac{d}{dz}\int_0^R n\rho(v+v_{Tz})r dr \qquad (21)$$

This deposition rate having a unit of m/s has a meaning similar to so-called deposition velocity (particle flux towards a wall per unit concentration).

Figure 7 shows the change in the deposition rate in the axial direction. When the furnace temperature is 10°C, that is, the

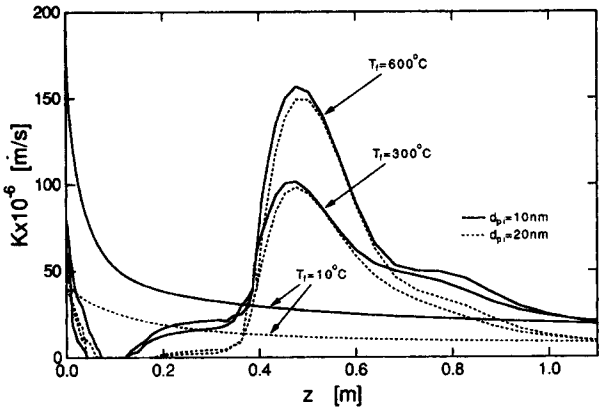

Figure 7. Change in deposition rate, K, in the axial direction of pipe.

flow in the pipe is isothermal, the deposition rates decrease with z. In this case, large deposition velocities found near $z=0$ are caused by large concentration gradient above the wall due to the uniform or nearly uniform concentration profile in the vicinity of the pipe inlet. For elevated temperatures of pipe wall, the deposition rates are quite small around the region where the wall is heated by the furnaces ($z_{f1}=0.09$ m $\le z \le z_{f2}=0.39$ m). The values of K begin to increase steeply and attain to their peaks after an aerosol passes through the heated region. The increase in K is attributable to thermophoresis because the aerosol in this cooling region is hotter than the pipe wall. The deposition rates approach to those for isothermal deposition as the axial coordinate further increases and the difference between the aerosol and wall temperature becomes smaller. Since Eqs. 19 and 21 give an another expression of P as:

$$P=1-\frac{2\pi R}{Q}\int_0^z K dz \tag{22}$$

the decrease in the numerically calculated values of P with increasing T_f is concluded to be mainly caused by the enhancement of deposition in the cooling region.

Change in particle size by evaporation

Besides the steady decrease in penetration discussed in the previous section, the measurements obtained at higher temperatures in Figure 4a show a steep decrease in the penetration which cannot be explained by the wall loss calculations. The steep decrease in penetration is found at different temperatures for Ag and NaCl particles and occurs at a lower temperature for smaller particle size. Reducing the gas flow rate in the pipe also shifts the temperature at which the decrease occurs lower, as shown in Figure 4b.

The material dependence of the temperature at which the penetration decreases steeply suggests that there is a change in the particles themselves. Figures 8a and 8b show the change in the particle-size distributions at the outlet of the pipe by the frequency against particle diameter. It is seen that the particle-size distributions shift toward smaller diameter as the furnace temperature increases. Ag particles observed with transmission electron microscopy were almost spherical and not agglomerated, but NaCl particles were not able to be examined due probably to evaporation by electron beam. The particle diameter at which the maximum frequency is found is recorded as the representative particle size at the pipe outlet, d_{po}. The ordinate of Figures 9a and 9b, which is the ratio of d_{po} to the particle size at the inlet, d_{pi}, indicates the diameter reduction ratio. Sharp decreases in the particle size are found at about the same temperature at which the steep changes in the penetration are found in Figure 4.

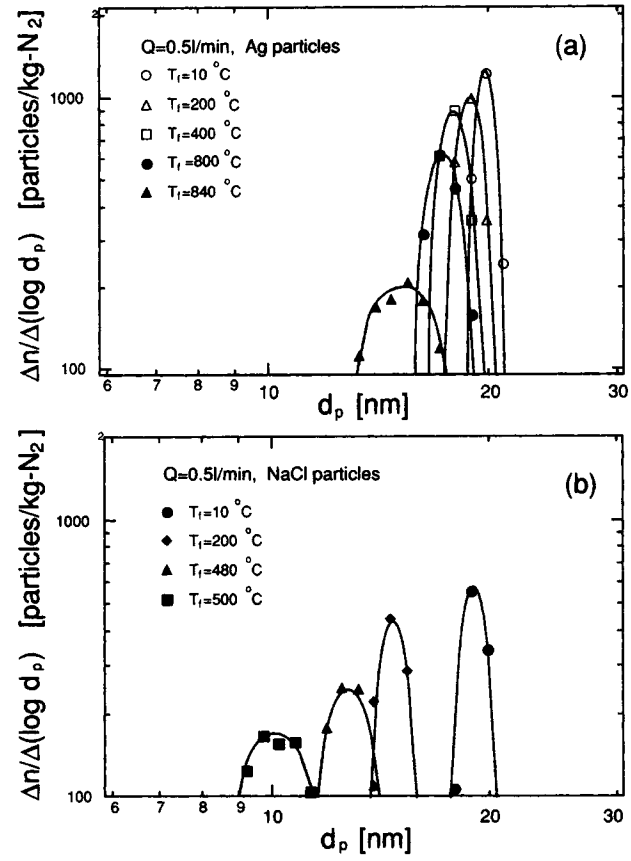

Figure 8. Particle-size distribution measured at the outlet of pipe: (a) Ag particles; (b) NaCl particles.

These figures reveal that the very fine particles evaporate or sublimate to reduce their size at a considerably lower temperature than the melting point of the bulk material (962°C for Ag and 801°C for NaCl) and the size reduction proceeds more significantly for smaller particles.

Comparison of particle evaporation with theory

In order to explain the size reduction of particles, the theoretical mass flux equation for evaporative mass transfer is applied to the particles suspended in the heated pipe flow. The equation for the mass flux, J[kg/(m^{2}s)], is related to the change in particle diameter with time, t, as:

$$\frac{d}{dt}\left(\rho_p \frac{\pi d_p^3}{6}\right) = -\pi d_p^2 J \tag{23}$$

where ρ_p is the particle density. The appropriate expression for

Table 1. Mass and Collision Diameter of Molecules used in Calculation

	m_i or m_j (kg)	σ_{ii} or σ_{jj} (nm)
N_2	4.652×10^{-26}*	0.380**
Ag	1.791×10^{-25}*	0.288†
NaCl	9.704×10^{-26}*	0.429‡

*CRC (1991).
**Reid et al. (1986).
†Chapman (1966).
‡Estimated by the method of Reid et al. (1986) using data of Mochinaga et al. (1969).

J in the above equation depends on whether the system considered is a continuum or not. When the mean free path of the molecules of evaporating species leaving the particle surface, λ_i, is large compared with the particle radius, that is, when the Knudsen number defined by $Kn_i=2\lambda_i/d_p$ is sufficiently large ($\gg 1$), the elementary kinetic theory of gases can be used to predict the mass flux.

The effective mean free path of evaporating species i (= Ag or NaCl in this study), λ_i, in the gas of species j ($=N_2$) is obtained from the kinetic theory of gases as:

$$\lambda_i=\frac{\kappa T}{\pi\sigma_{ij}^2 p(1+m_i/m_j)} \tag{24}$$

where m_i is the molecular mass of the species i. The collision diameter, σ_{ij}, for binary collisions between i and j molecules can be obtained using the following combining rule:

$$\sigma_{ij}=(\sigma_{ii}+\sigma_{jj})/2 \tag{25}$$

The values of m_i, m_j, σ_{ii} and σ_{jj} are listed in Table 1.

Preliminary calculations using Eqs. 24 and 25 showed that the value of Kn_i for the experimental conditions of this study ranged from about 3 to 40. Therefore, we use the flux expression for free-molecule evaporation.

Assuming that the vapor pressure of evaporating species far from the particle surface is zero because of an extremely small amount of vapor material in the pipe, the mass flux, J, in Eq. 23 is given by (Davis et al., 1980):

$$J=\frac{E\bar{c}_i m_i p_i^s}{4\kappa T} \tag{26}$$

where p_i^s is the vapor pressure immediately above the particle surface and the mean molecular speed $\bar{c}_i$ is calculated as:

$$\bar{c}_i=(8\kappa T/\pi m_i)^{1/2} \tag{27}$$

The evaporation coefficient, E, which accounts for the deviation of molecular velocities near the particle surface from the Maxwell-Boltzmann distribution, has not been fully established but has been found to be of order unity. We hence assumed $E=1$ in Eq. 26. The increase in the vapor pressure at the particle surface p_i^s due to particle curvature is related to the size and properties of the particle by the following Kelvin equation:

$$p_i^s=p_i^0\exp\left(\frac{4m_i\gamma}{\rho_p\kappa T d_p}\right) \tag{28}$$

where p_i^0 is the vapor pressure over a flat surface and γ is the surface tension of particle material. The values of ρ_p, p_i^0 and γ used in the calculation of Eq. 28 are given in Table 2 as functions of temperature.

The exact solution of Eq. 23 requires a great computational effort since the distribution of J and d_p in the radial and axial direction of the test pipe must be taken into account. However, the results of calculation described in the second section indicated that the gas temperature variation and the velocity in the axial direction were much larger than those in the radial direction. Therefore, we analyze Eq. 23 using average properties of the gas over a section of a pipe and compute the change in the particle diameter along the axial direction.

Rearrangement of Eq. 23 gives:

$$\frac{dd_p}{dz}=-\left(\frac{dz}{dt}\right)^{-1}\frac{2J}{\rho_p}=-\frac{2J}{\bar{v}(z)\rho_p} \tag{29}$$

where $\bar{v}(z)$, the average gas velocity over a pipe section at an axial position z, is defined by:

$$\bar{v}(z)=\frac{1}{\pi R^2}\int_0^R v(r,z)2\pi r dr \tag{30}$$

The average temperature,

$$\bar{T}(z)=\frac{1}{\pi R^2}\int_0^R T(r,z)2\pi r dr, \tag{31}$$

is also defined and used to describe J and ρ_p in Eq. 29 as functions of the position z.

After the computation of $\bar{v}(z)$ and $\bar{T}(z)$ are made with the calculation results of Eqs. 1-4, Eq. 29 is solved by the Runge-Kutta-Gill method to obtain d_p at the pipe outlet, that is, $d_{po}=d_p(z=Z)$.

The results calculated as described are shown in Figures 9a and 9b by the solid, dashed and chain lines. These lines explain

Table 2. Dependence of Surface Tension γ, Density ρ_p and Vapor Pressure p_i^0 of a Particle on Temperature T [°C]

	γ (N/m)	ρ_p (kg/m^3)	log p_i^0 (p_i^0 in (Pa))
Ag	$1{,}059.5\times10^{-3}-0.1362\times10^{-3}T$*	$9.911\times10^3-6.511\times10^{-1}T$**	$10.49-13{,}649/(T+273.15)$†
NaCl	$190.8\times10^{-3}-0.093\times10^{-3}T$*	$1.549\times10^3-0.5T$**	$10.91-14{,}255/(T+273.15)$‡

*Shiba (1949).
**Elliott and Gleiser (1960).
†CRC (1991).
‡Maissel and Glang (1970).

the dependence of the diameter reduction ratio upon the furnace temperature well. The predicted temperatures at which the particle size shows steep decreases are in good agreement for both Ag and NaCl particles. The difference between the temperatures for Ag and NaCl was found to be mainly resulted from the difference in the vapor pressure, p_i^s, in the mass flux expression, Eq. 26. The calculated results also give good predictions for the difference in the diameter reduction ratio due to the initial particle diameter (Figure 9a) and flow rate of the carrier gas (Figure 9b), indicating that the evaporative loss of solid particles at elevated temperatures (but below melting point) can be evaluated theoretically.

Discussion

Correlation of penetrations with dimensionless parameters

It is obvious from Figure 6 that the deposition rates, K, for two different particle sizes are fairly close to each other near their peaks although those for isothermal deposition differ considerably due to difference in Brownian diffusivity. In this section, the combined effect of thermophoresis and Brownian diffusion is investigated using dimensionless parameters. In most existing works concerned with nonisothermal deposition, arrangement of deposition rates or particle penetrations using dimensionless parameters have been done analytically or semi-empirically. However, it is very difficult to develop a nondimensional formula of deposition rates directly in this work, because the dependence of gas properties and particle diffusivity upon temperature are taken into account. Therefore, the numerical calculation results obtained here are rearranged using dimensionless parameters.

The effect of thermophoresis has been expressed by the following two parameters: one is $Pr_g\alpha$ where Pr_g is defined as $\mu C_p/\lambda$, the other is dimensionless temperature difference, θ^* $[=T_0/(T_f-T_0)]$. The gas properties appearing in the parameters are based on the average temperature T_m $[=0.5(T_0+T_f)]$. Stratmann and Fissan (1991) analyzed particle deposition due to convection and thermophoresis and derived a thermophoretic parameter as:

$$\beta=\frac{Pr_g\alpha+0.025}{\theta^*+0.28} \tag{32}$$

and approximated their theoretical calculation results by:

$$P_T(\beta)=\exp(-0.845\beta^{0.932}) \tag{33}$$

where P_T is the penetration due solely to thermophoresis. The effect of Brownian diffusive deposition is considered to be taken into account by a parameter, ζ, where $\zeta=Z/(RPe_p)$ with $Pe_p=2\bar{v}R/D$ and $\bar{v}$ being the average axial gas velocity at T_m, since the analytical solution for isothermal diffusive deposition, P_D, is expressed according to Gormley and Kennedy (1949) as:

$$\left.\begin{aligned}P_D(\zeta)&=1-4.07\zeta^{2/3}+2.40\zeta+\ldots \quad (\zeta<0.011),\\ P_D(\zeta)&=0.819\exp(-6.68\zeta)+0.0975\exp(-44.6\zeta)+0.0325\exp(-114\zeta)+\ldots \quad (\zeta\geq 0.011)\end{aligned}\right\} \tag{34}$$

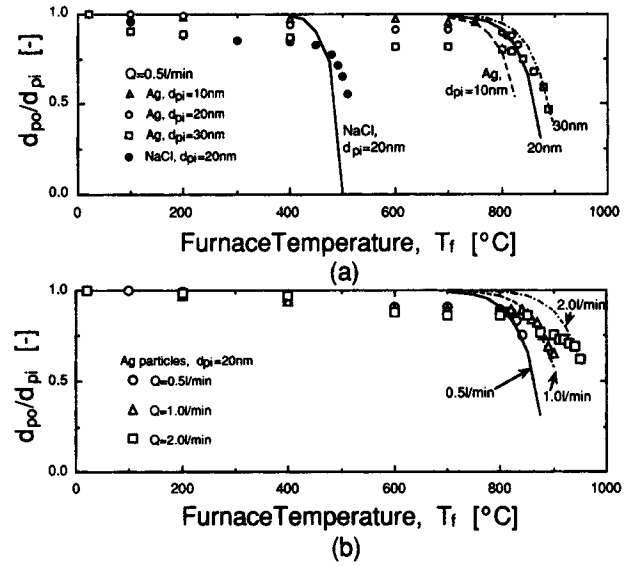

Figure 9. Diameter reduction ratio, d_{po}/d_{pi}, against furnace temperature for nonisothermal laminar flow.

Lines indicate the results from present calculation: (a) effect of particle size and material; (b) effect of flow rate of gas.

Correlation of the values of P obtained by the present numerical calculation using P_T and P_D revealed that P could not be expressed by any simple formula of P_T and P_D. Including a function of both β and ζ, the present calculations were found to be fitted well by:

$$P=P_T(\beta)P_D(\zeta)(1+1.54\zeta_0^{0.14}\beta)$$
$$(0\leq\beta\leq 7.2\times10^{-1},\quad 0\leq\zeta\leq 6.0\times10^{-2}) \tag{35}$$

where ζ and ζ_0 are evaluated based on the average and inlet temperatures, respectively. Figure 10 shows the comparison between Eq. 35 and the numerical calculation results, where the values of $P/[P_D(1+1.54\zeta_0^{0.14}\beta)]$ obtained with the numerical calculations (heavy line) agrees well with the dashed line, β vs. P_T by Eq. 33. The value of P in Eq. 35 approaches to P_T when ζ comes to zero and thus the effect of Brownian diffusion is absent, while it becomes P_D for isothermal deposition, that is, $\beta=0$. This correlation also suggests that the effect of thermophoretic deposition cannot be simply superposed to Brownian diffusive deposition, as described earlier.

Conditions for the numerical model for penetration

The model for prediction of penetration described earlier includes the conditions or assumptions that the flow in the pipe is laminar and that change in particle size and concentration due to coagulation and evaporation is negligible.

The first condition is needed because the equations for gas flow, temperature and particle concentration are derived for a steady-state laminar flow. Since the flow inside the heated

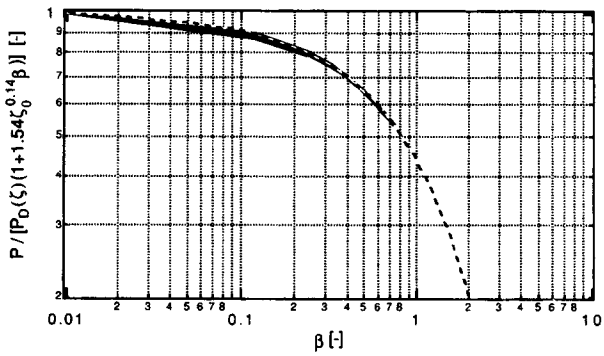

Figure 10. Correlation by dimensionless parameters for present calculations.

Heavy line represents the range of $P/[P_D(\zeta)(1+1.54\zeta_0^{0.14}\beta)]$ against β obtained from present numerical calculations ($0\le\beta\le0.72$, $0\le\zeta\le0.060$). Dashed line indicates penetration due solely to thermophoresis, β vs. $P_T(\beta)$, described in Eq. 33.

pipe could not be visualized due to the electric furnaces around the pipe, we estimated whether the flow is laminar or not by utilizing an empirical correlation in an existing literature (Metais and Eckert, 1964). The literature suggests that a heated or cooled vertical pipe flow is evaluated by a set of dimensionless parameters, $\psi = GrPr_g(2R)/L$ and Re, where Grashof number, $Gr[=g(\Delta T/T_m)(2R)^3/(\mu/\rho)^2]$, is based on the gas properties at the average temperature, T_m, difference between the inlet gas and the wall temperatures, $\Delta T(=T_f-T_0)$, and L is regarded as the length of the heated region $(z_{f2}-z_{f1})$. The values of ψ in this study are calculated to be in the range of $0\le\psi\le6.2\times10^2$. For the range of ψ a diagram presented in the literature suggests that the fluid flow is laminar (forced convection or forced and free (mixed) convection) when Re is smaller than about 2×10^3. Since the values of Re of this study range from 35 to 230, the flow is estimated to be laminar.

The effect of particle coagulation described in the second assumption is estimated for the present experimental conditions. The particle concentration, n_c^*, in the pipe necessary to change number concentration by 1% due to coagulation is estimated by the following equation (Hinds, 1982):

$$\frac{1}{(1+K_B' n_c^* t_r)} \ge 1-0.01 \tag{36}$$

where K_B' is the Brownian coagulation function and t_r is the particle residence time. The value of K_B' which is of the order of 10^{-15} m^3/s for the particle sizes of this study (Okuyama et al., 1984) and the maximum residence time of 29 s give the concentration n_c^* of about 3×10^{11} particles/m^3. Since the particle number concentration used in the experiments is below 5×10^9 particles/m^3, the effect of coagulation on penetration is negligible.

For particle evaporation, the measurements showed that the decrease in size of Ag particles ($d_{pi}=10$ and 20 nm) is less than 10% when the furnace temperature is lower than 700°C. The 10% change in particle size is found to shift the calculated penetration by at most 2%. In this case, the measured and calculated penetrations agree well as demonstrated, which validates the present calculation. However, slight decreases in particle size are found for NaCl particles at low furnace temperatures, as shown in Figures 8 and 9a. It follows that there may exist a low temperature region where diffusion, thermophoresis and evaporation are effective simultaneously. This might have caused the reduced accuracy of prediction of P for NaCl particles, as shown in Figure 4a.

To analyze such complicated problems, a comprehensive model in which all the particle dynamics (diffusion, thermophoresis and evaporation) are taken into account is thought to be useful. However, an analysis in which particles are transported by convection, diffusion and thermophoresis while changing their size by evaporation is extremely complicated and requires a huge computational effort because calculations of both concentration and size distribution throughout the inner space of the pipe are needed. In this study, therefore, the analysis of particle-size reduction is simplified to be less coupled with diffusion and thermophoresis since the effect of evaporation is evidently predominant in a particular temperature region. Although the comprehensive model would be very interesting and important, development of the model should be a future task.

Summary

The depositional and evaporative losses of solid particles in a nonisothermal flow field have been investigated and the following results have been obtained.

(1) Analyses of particle concentration distribution including nonisothermal fluid flow calculation can predict the enhancement of the particle depositional loss at elevated wall temperature. It is found that the thermophoretic migration and the dependence of Brownian diffusivity on temperature considerably affect the rate of the depositional loss.

(2) Particles in a heated gas show reduction of their size below the melting point of the particle material. The change in particle size is satisfactorily explained with the theory for the evaporation in the free-molecule region.

Acknowledgment

Part of this work was supported by Saneyoshi Scholarship Foundation, CVD project research of The Society of Chemical Engineers, Japan, a Grant-in-Aid for Scientific Research on Priority Areas, Micro Heat Transfer in Materials Processing, from the Ministry of Education, Culture and Science of Japan (No. 05239207), and a Grant-in-Aid for Encouragement of Young Scientists from the Ministry of Education, Culture and Science of Japan (No. 05750673).

Notation

a = constant in Eq. 9
$\bar{c}_i$ = mean molecular speed, ms^{-1}
C_c = Cunningham correction factor
C_p = specific heat of gas, J·mol^{-1}·K^{-1}
d_p = particle diameter, m
d_{pi} = particle diameter at the pipe inlet, m
d_{po} = particle diameter at the pipe outlet, m
D = Brownian diffusivity of particles, m^2·s^{-1}
E = evaporation coefficient
Gr = Grashof number $(=g(\Delta T/T_m)(2R)^3/(\mu/\rho)^2)$
g = gravitational acceleration, m·s^{-2}
J = mass flux, kg·m^{-2}·s^{-1}
k = thermal conductivity of gas, W·m^{-1}·K^{-1}
k_p = thermal conductivity of particles, W·m^{-1}·K^{-1}
K = deposition rate, m·s^{-1}
K_B' = Brownian coagulation function, m^3·s^{-1}
Kn = Knudsen number
Kn_i = Knudsen number for evaporating species

L = length of heated region ($=z_{f2}-z_{f1}$), m
m_i = molecular mass of evaporating species, kg
m_j = molecular mass of gas species, kg
n = particle number concentration, particles (kg of carrier gas)$^{-1}$
n_c^* = particle concentration necessary to change concentration by 1% due to coagulation, particles$\cdot$m^{-3}
n_i = particle concentration at pipe inlet, particles (kg of carrier gas)$^{-1}$
n_i^* = particle number concentration at pipe inlet, particles$\cdot$m^{-3}
n_o^* = particle number concentration at pipe outlet, particles$\cdot$m^{-3}
n_w = particle concentration on wall surface, particles (kg of carrier gas)$^{-1}$
p = pressure, Pa
p_i^0 = vapor pressure over a flat surface, Pa
p_i^s = vapor pressure immediately above particle surface, Pa
P = particle penetration
P_D = particle penetration due to Brownian diffusion
P_T = particle penetration due to thermophoresis
Pe_p = Peclet number for particle ($=2\bar{v}R/D$)
Pr_g = Prandtl number for gas ($=\mu C_p/\lambda$)
Q = volumetric flow rate, m$^3\cdot$s^{-1}
r = radial distance, m
R = radius of pipe, m
Re = Reynolds number ($=2\bar{v}R\rho/\mu$)
t = time, s
t_r = residence time of particles in pipe, s
T = temperature, K
$\bar{T}$ = average temperature over a pipe section at an axial position z, K
T_0 = temperature at pipe inlet, K
T_f = furnace temperature, K
T_m = average temperature ($=0.5(T_0+T_f)$), K
T_w = wall temperature, K
u = radial velocity component, m$\cdot$s^{-1}
v = axial velocity component, m$\cdot$s^{-1}
$\bar{v}$ = average gas velocity over a pipe section, m$\cdot$s^{-1}
v_{Tr} = thermophoretic velocity in the radial direction, m$\cdot$s^{-1}
v_{Tz} = thermophoretic velocity in the axial direction, m$\cdot$s^{-1}
z = axial distance, m
z_{f1}, z_{f2} = axial positions of the ends of heated furnaces, m
Z = pipe length, m

Greek letters

α = thermophoretic coefficient
β = parameter for thermophoretic deposition
γ = surface tension of a particle, N$\cdot$m^{-1}
ΔT = difference between gas and wall temperatures ($=T_f-T_0$), K
ζ = parameter for Brownian diffusive deposition
ζ_0 = ζ for temperature of pipe inlet
θ^* = dimensionless temperature difference ($=T_0/(T_f-T_0)$)
κ = Boltzmann constant, J$\cdot$K^{-1}
λ = mean free path of gas molecules, m
λ_i = mean free path of molecules of evaporating species, m
μ = viscosity of gas, Pa$\cdot$s
ρ = density of gas, kg$\cdot$m^{-3}
ρ_i = gas density at pipe inlet, kg$\cdot$m^{-3}
ρ_p = density of particles, kg$\cdot$m^{-3}
σ_{ii} = collision diameter of evaporating species, m
σ_{ij} = collision diameter of binary collision between i and j, m
σ_{jj} = collision diameter of gas species, m
Φ_0 = function describing concentration profile
ψ = dimensionless parameter describing flow in pipe ($=GrPr_g(2R)/L$)

Literature Cited

Adachi, M., K. Okuyama, Y. Kousaka, S.-W. Moon, and J. H. Seinfeld, "Facilitated Aerosol Sizing Using the Differential Mobility Analyzer," *Aerosol Sci. Technol.*, **12**, 225 (1990).

Bird, R. B., W. E. Stewart, and E. N. Lightfoot, *Transport Phenomena*, Wiley International, New York (1960).

Chapman, T. W., "The Viscosity of Liquid Metals," *AIChE J.*, **12**, 395 (1966).

CRC (1991-1992), *Handbook of Chemistry and Physics* (55th ed.), Chemical Rubber Co., Cleveland (1991).

Davies, C. N., "Definitive Equation for the Fluid Resistance of Spheres," *Proc. Phys. Soc.*, **57**, 259 (1945).

Davies, E. J., P. Ravindran, and A. K. Ray, "A Review of Theory and Experiments on Diffusion from Submicroscopic Particles," *Chem. Eng. Commun.*, **5**, 251 (1980).

Elliott, J. F., and M. Gleiser, *Thermochemistry for Steel Making*, Vol. I, Addison-Wesley, New York (1960).

Gormley, P. G., and M. Kennedy, "Diffusion from a Stream Flowing through a Cylindrical Tube," *Proc. Roy. Ir. Acad.*, **52**, 163 (1949).

Hinds, W. C., *Aerosol Technology*, John Wiley & Sons, New York (1982).

Knudsen, J. G., and D. L. Katz, *Fluid Dynamics and Heat Transfer*, McGraw-Hill, New York (1958).

Kousaka, Y., K. Okuyama, M. Adachi, and T. Mimura, "Effect of Brownian Diffusion on Electrical Classification of Ultrafine Particles in Differential Mobility Analyzer," *J. Chem. Eng. Japan*, **19**, 401 (1986).

Maissel, L. I., and R. Glang, *Handbook of Thin Film Technology*, McGraw Hill, New York (1970).

Metais, B., and E. R. G. Eckert, "Forced, Mixed and Free Convection Regimes," *J. Heat Transfer*, **86**, 295 (1964).

Mochinaga, J., K. Cho, R. Takagi, and T. Kuroda, "Densities and Equivalent Conductivities of Fused UCl_3 and UCl_3-KCl Systems," *Denki Kagaku*, **37**, 654 (1969).

Montassier, N., D. Boulaud, and A. Renoux, "Experimental Study of Thermophoretic Particle Deposition in Laminar Tube Flow," *J. Aerosol. Sci.*, **22**, 677 (1991).

Okuyama, K., Y. Kousaka, and K. Hayashi, "Change in Size Distribution of Ultrafine Aerosol Particles Undergoing Brownian Coagulation," *J. Colloid Interface Sci.*, **101**, 98 (1984).

Patankar, S. V., *Numerical Heat Transfer and Fluid Flow*, McGraw-Hill, New York (1980).

Pratsinis, S. E., and K.-S. Kim, "Particle Coagulation, Diffusion and Thermophoresis in Laminar Tube Flows," *J. Aerosol Sci.*, **20**, 101 (1989).

Rader, D. J., P. H. McMurry, and S. Smith, "Evaporation Rates of Monodisperse Organic Aerosols in the 0.02- to 0.2-μm-Diameter Range," *Aerosol Sci. Technol.*, **6**, 247 (1987).

Reid, R. C., J. M. Prausnitz, and B. E. Poling, *The Properties of Gases and Liquids* (4th ed.), McGraw Hill, New York (1986).

Schmidt-Ott, A., "New Approaches to *in situ* Characterization of Ultrafine Agglomerates," *J. Aerosol Sci.*, **19**, 553 (1989).

Shiba, K., *Butsuri Jousuu Hyou* (4th ed.), Iwanami, Tokyo (1949).

Stratmann, F., and H. Fissan, "Convection, Diffusion and Thermophoresis in Cooled Laminar Tube Flow," *J. Aerosol Sci.*, **19**, 793 (1988).

Stratmann, F., and H. Fissan, "Experimental and Theoretical Study of Submicron Particle Transport in Cooled Laminar Tube Flow due to Combined Convection, Diffusion, and Thermophoresis," *J. Aerosol Sci.*, **20**, 899 (1989).

Stratmann, F., and H. Fissan, "Nondimensional Investigation of Submicron Particle Transport in Cooled Laminar Flow," *J. Aerosol Sci.*, **22**, S211 (1991).

Talbot, L., R. K. Cheng, R. W. Schaefer, and D. R. Willis, "Thermophoresis of Particles in a Heated Boundary Layer," *J. Fluid Mech.*, **101**, 737 (1980).

Walker, K. L., G. M. Homsy, and F. T. Geyling, "Thermophoretic Deposition of Small Particles in Laminar Tube Flow," *J. Colloid Interface Sci.*, **69**, 138 (1979).

Manuscript received Oct. 13, 1992, and revision received Mar. 29, 1993.